Far-infrared investigations of strained PbTe

J. Oswald and P. Pichler
Institut für Physik, Montanuniversitat Leoben, A-8700 Leoben, Austria

B. B. Goldberg
Department of Physics, Boston University, 590 Commonwealth Avenue, Boston, Massachusetts 02215

G. Bauer
Institut für Halbleiterphysik, Universitat Linz, A-4040 Linz, Austria
(Received 12 August 1993; revised manuscript received 8 December 1993)

Far-infrared magnetotransmission of strained epitaxially grown n-type PbTe was investigated using experiments in the Faraday ($\mathbf{B} \parallel [111]$) and Voigt ($\mathbf{B} \parallel [1\bar{1}0]$) configurations. The analysis of the data is based on a complete frequency-dependent dielectric function for both magnetic-field configurations, taking into account explicitly the effects of the strain splitting of the four L states in the Brillouin zone. The experiments were performed at temperatures ranging from 1.4 K to 20 K and the dependence of the Fermi energy on magnetic field, temperature, as well as the strain splitting were calculated within the Mitchell-Wallis $\mathbf{k} \cdot \mathbf{p}$ scheme. It is shown that this method is capable of determining strain-induced shifts of equivalent L states with an accuracy of about 0.5 meV. These techniques are applicable to other strained many-valley systems such as Si/SiGe.

I. INTRODUCTION

Lead telluride and its pseudobinary alloys have been of considerable interest for the fabrication of mid-infrared p-n junction lasers and infrared detectors.[1] Twelve years ago good quality epitaxial films became available, grown either by hot wall epitaxy[2] or by molecular beam epitaxy.[1] Since bulk PbTe usually has carrier concentrations of the order of 10^{17} cm^{-3} or more, insulating substrate material is unavailable. Thus epitaxial films were deposited on insulators such as BaF_2, KCl, or NaCl for transport and optical investigations.[3] Although these substrates are transparent in wide regions of the mid-infrared and far-infrared regions of the electromagnetic spectrum, they have two major disadvantages. First, there is a considerable lattice mismatch between the substrate and film, e.g., BaF_2 and PbTe.[3] Second, the temperature dependence of the thermal expansion coefficients differ considerably.[4] Consequently, at temperatures around 77 K and even more so at 4.2 K where optical and transport investigations are usually performed, the substrate induced strain has a major influence on the electronic properties of the PbTe films. This is especially true for the growth on cleaved BaF_2 substrates where growth proceeds along the [111] direction.

PbTe is a semiconductor with both the conduction and valence band extrema located at the L points of the Brillouin zone and the surfaces of constant energy are approximately ellipsoids of revolution along the four $\langle 111 \rangle$ directions.[5,6] The differential contraction between the comparatively thin PbTe epitaxial film grown at temperatures from 550 K to 650 K and the BaF_2 substrate produces biaxial tensile strain in the PbTe film which lifts the fourfold degeneracy of the L states. This phenomenon is well documented in the literature. The strain splitting shifts the [111] valley in the conduction band which has its main axis oriented parallel to the growth direction downward in energy with respect to the three remaining valleys oriented with their main axes obliquely ($\theta = 70.53°$) to the growth direction (Fig. 1). In the valence band a similar splitting occurs with the three obliquely oriented valleys lying higher than the longitudinal [111] valley.

This strain splitting of the L states has been observed by a variety of transport and optical experiments. Methods such as weak field magnetoresistance,[7,8] quantum magnetoresistance[9,10] (Shubnikov–de Haas effect), interband emission,[11] far-infrared cyclotron resonance,[12–19] and interband magneto-optics[20] have been used. The experiments relying on intraband phenomena make use of the different population of the four valleys as a consequence of their strain splitting ΔE. Using x-ray diffraction the amount of strain present in the samples has been investigated not only at room temperature but also down to $T = 25$ K.[21] Several authors have reported quite different values for ΔE from about 10 meV down to 1 meV (for the conduction band). This problem is complicated since precise data on ΔE for either the conduction or the valence band require a careful analysis of depopulation effects in the four L valleys and thus a quite elaborate comparison of experimental data with calculations. Further complications arise from the fact that work hardening occurs in PbTe films grown on BaF_2 substrates which are subjected to repeated thermal cycling from room temperature to cryogenic temperatures ($T = 77$ and 4.2 K) and back. Asch *et al.*[22] have reported that the biaxial tensile strain alters considerably in the first few thermal cycles.

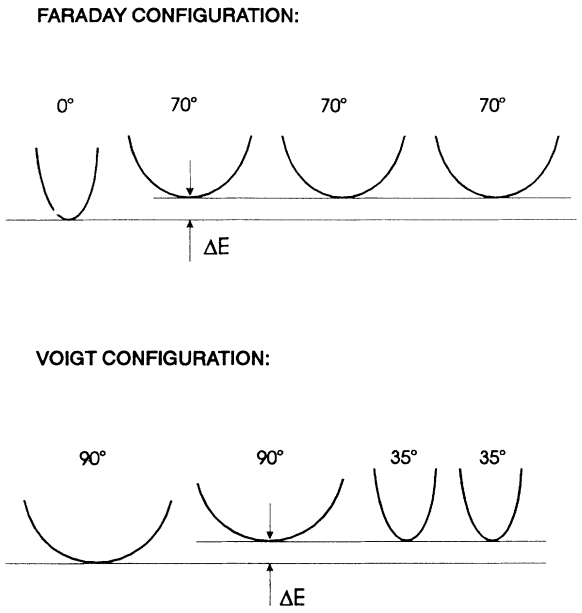

FIG. 1. Schematic diagram of the strain splitting of the conduction band valleys for biaxial tensile strain in the (111) growth plane for Faraday and Voigt configurations. The angles between the direction of the applied magnetic field and the main axes of the four surfaces of constant energy in k space are given. l and o refers to longitudinal and oblique with respect to the [111] growth direction. ΔE indicates the energy due to the lifting of the degeneracy because of biaxial tensile strain.

In this paper we show that far-infrared (FIR) magnetotransmission is useful for studying the depopulation effects in the strain split L valleys if more than one configuration of the magnetic field with respect to the growth direction is employed. However, for the analysis of the data a complete model dielectric function is necessary. We show that ΔE can be determined with an uncertainty of about 0.5 meV using far infrared magneto-optics. The structure of this paper is as follows. Experimental details are presented in Sec. II. In Sec. III we present the calculation of the Fermi energy for a given carrier concentration as a function of ΔE, temperature, and the direction of the magnetic field using the Mitchell-Wallis band structure model.[5,23] Furthermore, we present the magnetic-field dependence of the dielectric function both for Faraday and Voigt geometries including the strain splitting in detail. The method presented is in principle also useful for far infrared studies in other strained, many-valley systems such as Si/SiGe, etc. In Sec. IV we present the data and analysis of the experimental magnetotransmission spectra, and in Sec. V the main conclusions are summarized.

II. EXPERIMENT

Far infrared investigations of a PbTe film grown on [111] oriented BaF_2 were performed using a CO_2 laser pumped FIR methanol laser using the energies provided by the methanol molecule. The three different laser lines utilized were $\lambda = 118.8$, 96.5, and 70.65 μm. The laser radiation was guided with a light pipe system from the laser to the sample. The experiments were performed with the sample mounted in a He exchange gas chamber inserted into the magnet system so that its temperature could be varied from 1.4 K to 20.2 K. The sample was mounted either in Faraday geometry ($\mathbf{B} \parallel \mathbf{k} \parallel [111]$) and illuminated with unpolarized radiation, or Voigt configuration ($\mathbf{B} \perp \mathbf{k} \parallel [111]$, $\mathbf{B} \parallel [1\bar{1}0]$) using linearly polarized radiation provided by a FIR polarizer mounted at low temperatures just above the sample. The incident radiation was split by a Ge beam splitter above with sample, with about half passing through and half around the sample. Both beams were detected by bolometers held at 1.2 K, located below the magnetic field region. The total signal was the ratio of the sample transmitted beam and the unperturbed beam, effectively canceling out any fluctuations in laser power. FIR spectra were taken at fixed laser wavelength while sweeping the magnetic field. The sample had a carrier concentration of $n = 1 \times 10^{16}$ cm^{-3} and a mobility $\mu = 520\,000$ cm^2/V s at $T = 4.2$ K.

III. THEORY

For PbTe samples grown epitaxially on (111) substrates, the only possible orientation of the magnetic field for Faraday configuration is ($\mathbf{B} \parallel [111]$), i.e., parallel to the growth axis, because of geometrical reasons. For epitaxial layers, and normal incidence of the FIR radiation, the magnetic field has to be perpendicular to the growth direction, i.e., in the plane of the epitaxial layer. Consequently, any direction $[hkl] \perp [111]$ is possible. Because of the many-valley band structure the simplest situation occurs when the magnetic field is oriented parallel to a $[1\bar{1}0]$ direction. For this direction two valleys are oriented with their main axis under an angle of $\theta = 35.26°$ and the two others under $\theta = 90°$. In Faraday configuration ($\mathbf{B} \parallel [111]$) these angles are $\theta = 0°$ (one longitudinal valley l) and $\theta = 70.53°$ (three oblique valleys o).

A. Landau levels and Fermi energy versus magnetic field

Knowledge of the occupancy of the initial and final Landau states is necessary for the full interpretation of magneto-optical data. For PbTe epitaxial films with $\mathbf{B} \parallel [111]$ or $\mathbf{B} \parallel [1\bar{1}0]$, transfer of electrons between the Landau states occurs as a function of magnetic field and temperature. In addition, the initial occupancies of the different valleys depend also on the induced strain of the samples since the biaxial tensile strain present at low temperature lifts the degeneracy of the four valleys.[10] The Landau level energies presented here were calculated using a (4×4) matrix Hamiltonian[23,24] with the band parameters as listed in Table I.

In Fig. 2 the dependence of Landau level energies on applied field is shown for $\mathbf{B} \parallel [111]$ for three different values of the biaxial tensile strain. The energy shifts between the three oblique valleys and the longitudinal val-

TABLE I. Band parameters of PbTe in Mitchell-Wallis notation; see Ref. 28.

E_g	$2P_\perp^2/m_0$	$P_\perp/P_\parallel$	m_t^-/m_0	m_l^-/m_0	m_t^+/m_0	m_l^+/m_0	g_t^-	g_l^-	g_t^+	g_l^+
189.7 meV	6.02	3.42	+0.06	0.505	−0.102	−0.92	−1.39	−1.72	+4.39	+2.61

ley for these tensile strains are $\Delta E = 0$ meV [Fig. 2(a)], 1.5 meV [Fig. 2(b)], and 5 meV [Fig. 2(c)]. The dependence of the Fermi energy on magnetic field is quite sensitive to these shifts, in particular if the Fermi energy is comparable with ΔE, which is the case for the sample investigated (E_F=2.5 meV). The calculation of the Fermi energy as a function of B used the condition that the total number of carriers does not vary in the field and temperature range investigated:

$$n_{\rm tot} = \frac{1}{4\pi^2}\frac{eB}{h}\sum_{n,\sigma}\int_{-\infty}^{\infty} f(E^v_{n,k_B,\sigma,E_F,T})(dk_B), \qquad (1)$$

where the summation extends over the four valleys (v), n and s denote the Landau and spin quantum number, k_B is the carrier momentum along the B direction, E_F is the Fermi energy, and f is the Fermi-Dirac distribution function.

For clarity and simplicity the Landau level indices for the longitudinal (l) and oblique (o) valleys are given only in Fig. 2(b). The resonant magnetic fields where cyclotron resonance transitions in these two Landau ladders occur are indicated for laser wavelengths $\lambda = 70.65$ μm and 118.85 μm. The variation of E_F shown results from Eq. (1).

Figure 3 shows the Landau levels in Voigt configuration $\mathbf{B} \parallel [1\bar{1}0]$ for $\Delta E = 1.5$ meV in analogy to Fig. 2(b). The biaxial strain lifts the degeneracy of the two valleys with $\theta = 90°$, consequently three valleys are shifted upwards in energy, two valleys with $\theta = 35.26°$ and one valley with $\theta = 90°$. The transitions for $\lambda = 96.55$ μm have been added as well as a spin-flip transition for the $\theta = 90°$ valley.

In such a strained many-valley system, the population of one particular valley changes with magnetic field and temperature. For the interpretation of the strength of magneto-optical resonances these variations have to be known.

Figure 4 shows the occupancy of the lowest Landau level ($\theta = 0°$) of the (111) valley as a function of B for $\mathbf{B} \parallel [111]$ at several temperatures. The increase of the occupancy for $n, \sigma = 0_l^-$ at low fields results from the

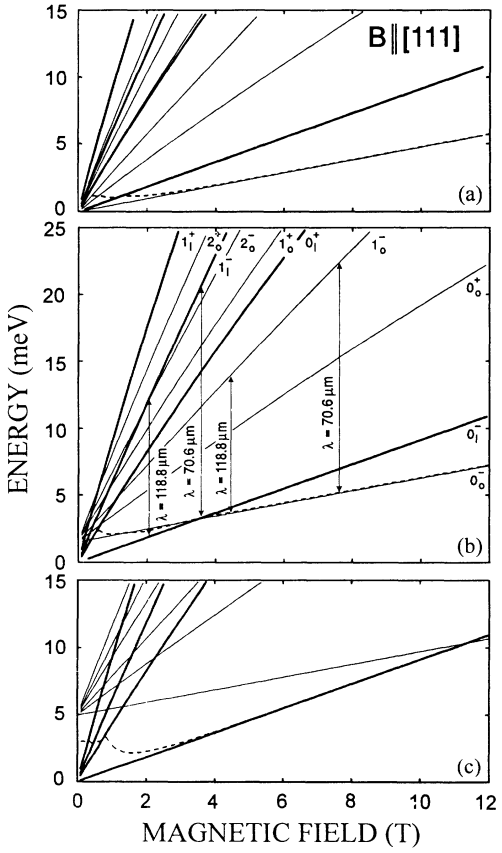

FIG. 2. Calculated Landau levels versus magnetic field ($\mathbf{B} \parallel [111]$) using the band parameters of Table I. The bold lines correspond to Landau levels of the longitudinal (l valley), and the fainter ones to those of the three oblique valleys (o valley). (a) Strain splitting $\Delta E = 0$ meV, (b) $\Delta E = 1.5$ meV, and (c) $\Delta E = 5$ meV. The dashed line shows the variation of the Fermi level E_F with magnetic field at $T = 0$ K. The arrows indicate positions of resonant magnetic fields for cyclotron resonance transitions within the l and o valleys for two FIR laser photon energies.

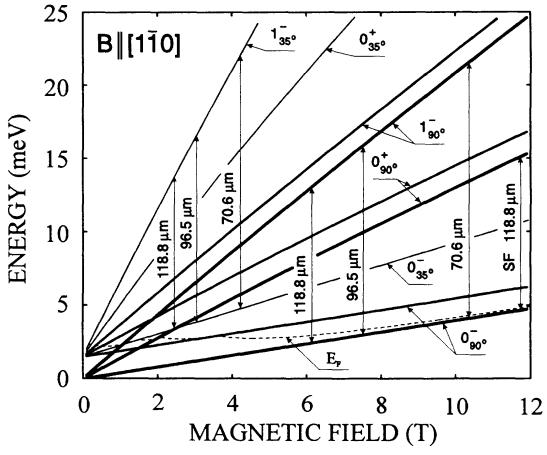

FIG. 3. Calculated Landau levels versus magnetic field for $\mathbf{B} \parallel [1\bar{1}0]$ with a strain splitting energy of $\Delta E = 1.5$ meV. Bold lines correspond to Landau levels of the two valleys for which $\theta = 90°$ (the lower set of Landau levels is for the l valley, shifted parallel by 1.5 meV relative to one of the o valleys) and the fainter lines to those for which $\theta = 35.26°$. The magnetic field dependence of the Fermi energy is shown by the dashed line. Several cyclotron resonance transitions for three different FIR laser photon energies are shown (corresponding to $\lambda = 118.8$ μm, $\lambda = 96.5$ μm and $\lambda = 70.6$ μm) and one spin flip transition within the $\theta = 90°$, l valley for $\lambda = 118.8$ μm.

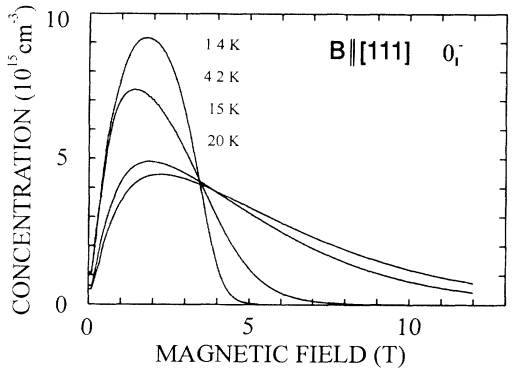

FIG. 4. Calculated carrier concentration in the lowest Landau level (0_l^-) as a function of magnetic field (**B** ‖ [111]) for four temperatures for the n-PbTe sample with $n = 1 \times 10^{16}$ cm^{-3} assuming a strain splitting energy of $\Delta E = 1.5$ meV.

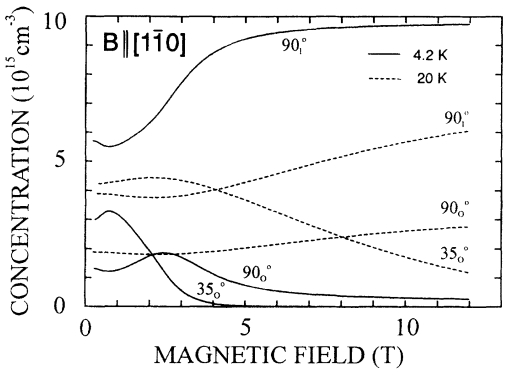

FIG. 5. Calculated carrier concentration in the lowest (0^-) Landau levels of different valleys versus magnetic field (**B** ‖ [1$\bar{1}$0]) for the $\theta = 90°$ l valley, the $\theta = 90°$ o valley, and in the two $\theta = 35°$ o valleys, for the temperatures 4.2 K and 20 K. For sufficiently high magnetic fields most of the carriers are in the lowest Landau level of the $\theta = 90°$ l valley.

fact that the higher Landau levels become depopulated. At a field between 3 and 4 T [see Fig. 2(b)] an intersection of the 0_l^- and 0_o^- levels occurs and the lowest lying level is then the $n = 0_o^-$ level and consequently the occupancy of $n, \sigma = 0_l^-$ level decreases. With increasing temperature, the thermal activation of carriers reduces the transfer of electrons out of the $n, \sigma = 0_l^-$ level in the higher field region, whereas in the lower field region the thermal activation depopulates the $n, \sigma = 0_l^-$ level. The transitions between these two regimes depends critically on the magnitude of the strain induced shift ΔE.

For the **B** ‖ [1$\bar{1}$0] configuration, the transfer of the carriers as a function of magnetic field is shown in Fig. 5 for the temperatures 2 K and 20 K. The symbols l and o denote the valleys oriented with their main axis parallel (l) or oblique (o) to the growth direction and the angles refer to their orientation with respect to the magnetic field. For the highest fields the lowest lying state [$0_{90°}^-(l)$; see Fig. 4] has the largest occupancy. With increasing temperature this occupancy decreases whereas the other Landau levels, especially also those of the $\theta = 35.26°$ Landau ladders become populated.

B. Magnetic-field dependence of the dielectric function

In the following, expressions for the classical dielectric function in the many-valley semiconductor are given where the strain splitting of otherwise equivalent valleys is explicitly taken into account.

1. *Faraday configuration B ‖ [111]*

Two cyclotron resonances occur due to carriers in the longitudinal and the three oblique valleys which contribute to the free carrier susceptibility for $\chi_{\rm FC}^{\pm}$ for the two circular polarizations: $\chi_{\rm FC}^{\pm} = \chi_{\rm FC}^{\pm}(l) + \chi_{\rm FC}^{\pm}(o)$. For the longitudinal valley this contribution is[18,25]

$$\chi_{\rm FC}^{\pm}(l) = \frac{-n^l(\frac{e^2}{\epsilon_0})(\frac{1}{m_t})(\omega \pm \omega_{c1} - i\omega_{\tau 1})}{4\omega[(\omega \pm \omega_{c1})^2 + \omega_{\tau 1}]^2}, \tag{2}$$

where $\omega_{c1} = eB/m_t$, $\omega_{\tau 1}$ is a damping parameter, and n^l is the total carrier concentration in the longitudinal valley. In this classical dielectric function the distribution of the carriers among various Landau states of this valley is not taken into account. For the sample under investigation just the lowest lying 0_l^- state is populated at resonant fields for all three laser photon energies (see Fig. 2). The second contribution results from the three oblique valleys:

$$\chi_{\rm FC}^{\pm}(o) = \frac{-(4n^o\frac{e^2}{\epsilon_0 3m_0})[a(\omega + i\omega_{\tau 2}) \pm b\omega_{c1}](\omega^2 - \omega_{c2}^2 - \omega_{\tau 2}^2 - 2i\omega\omega_{\tau 2})}{\omega[(\omega^2 - \omega_{c2}^2 - \omega_{\tau 2}^2)^2 + 4\omega^2\omega_{\tau 2}^2]}, \tag{3}$$

where n^o is the total concentration of the carriers in the three oblique valleys,

$$\omega_{c2} = \frac{eB}{\left[\frac{1}{9m_t}(\frac{8}{m_l} + \frac{1}{m_t})\right]^{1/2}},$$

$$a = \frac{1}{12}\left(\frac{4}{m_l} + \frac{5}{m_t}\right)m_0,$$

$$b = \frac{1}{12}\left(\frac{8}{m_l} + \frac{1}{m_t}\right)m_0, \tag{4}$$

and $\omega_{\tau 2}$ is the damping parameter for the oblique valleys. Despite the fact that classical susceptibility expressions are used, the numerical results from Eq. (1) are used for the population for the two kinds of valleys.

2. *Voigt configuration B ‖ [1$\bar{1}$0]*

For the Voigt configuration, the situation is much more complicated since the strain splits two valleys which are

equivalent with respect to applied field. In Fig. 6 the orientation of the four valleys with respect to the applied magnetic field is shown. For convenience, the valleys are numbered 1 ($\theta = 90°$, lowest lying valley, corresponds to the longitudinal valley with respect to growth direction), 2 ($\theta = 90°$, shifted upwards by ΔE with respect to 1, corresponds to an oblique valley), and 3 and 4 ($\theta = 35.26°$, both valleys shifted by ΔE upwards with respect to 1, oblique valleys). The contribution from the carriers in these valleys to the free carrier susceptibility depends in addition on the orientation of the electric field of the radiation with respect to the magnetic field. For the ordinary mode, $\mathbf{E} \parallel \mathbf{B}$ the results are given in Refs. 19 and 25–27. Since in this paper most of the experimental data were taken in the $\mathbf{E} \perp \mathbf{B}$ configuration (extraordinary mode) the expressions for this configuration will be given in a form where strain splitting of the valleys can be accounted for. In the sample coordinate system the complex refractive indices $\tilde{n}$ are given by[19]

$$\tilde{n}_o^2 = \epsilon_{xx}, \tag{5}$$

$$\tilde{n}_e^2 = \frac{\epsilon_{yy} - \epsilon_{yz}\epsilon_{zy}}{\epsilon_{zz}}, \tag{6}$$

where o and e refer to ordinary and extraordinary modes and the ϵ_{ij} are components of the total dielectric tensor in this reference frame ($z \parallel [111]$).

The principal procedure has been outlined in several references. One starts with a classical equation of motion of carriers in the external $\mathbf{B}$ field and oscillatory $\mathbf{E}$ field and calculates in the coordinate system of one valley (see Fig. 6) the conductivity tensor which relates to $\epsilon = i\hat{\sigma}/\epsilon_0\omega$. The next step is a coordinate transformation into the sample axis coordinate system ($z \parallel [111]$, $x \parallel [1\bar{1}0]$, $y \parallel [11\bar{2}]$). For valley 1 the tensor components are given by

$$\epsilon^1(1,1) = -\frac{n^l e^2}{m_t \epsilon_0 \omega}\left(\frac{1}{\omega + i\omega_{\tau 1}}\right),$$

$$\epsilon^1(2,2) = -\frac{n^l e^2}{\epsilon_0 \omega m_t}\frac{\omega + i\omega_\tau}{[(\omega + i\omega_\tau)^2 - \omega_{cA}^2]},$$

$$\epsilon^1(3,3) = -\frac{n^l e^2}{\epsilon_0 \omega m_t}\frac{(\omega + i\omega_\tau)\left(\frac{m_t}{m_l}\right)}{[(\omega + i\omega_\tau)^2 - \omega_{cA}^2]},$$

$$\epsilon^1(2,3) = -\frac{in^l e^2}{\epsilon_0 \omega m_t}\frac{\left(\frac{9B}{m_l}\right)}{[(\omega + i\omega_\tau)^2 - \omega_{cA}^2]},$$

$$\epsilon^1(3,2) = -\frac{in^l e^2}{\epsilon_0 \omega m_t}\frac{\left(\frac{9B}{m_l}\right)}{[(\omega + i\omega_\tau)^2 - \omega_{cA}^2]}, \tag{7}$$

where all other ϵ elements are zero and

$$\omega_{cA} = \frac{eB}{(m_t m_l)^{1/2}}. \tag{8}$$

For the valley 2 ($\theta = 90°$) the carrier concentration according to Fig. 5 for $0_{90°}^{-}(o)$ has to be taken into account for our calculations which will be referred to in the following as $n_{90°}^{o}$, where o stands for oblique and 90° for the angle θ (see also Fig. 6). The tensor contributions are given by (in the sample coordinate system)

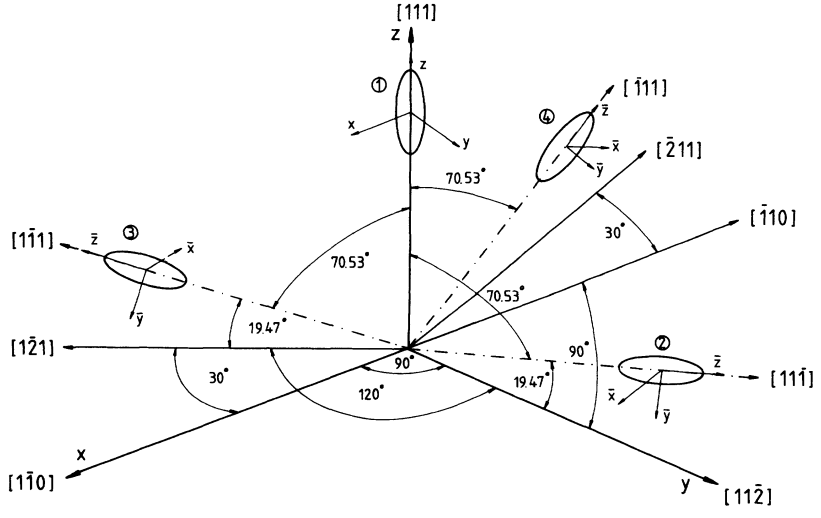

FIG. 6. Schematic diagram showing the surfaces of constant energy for electrons and holes along the four ⟨111⟩ directions and the coordinate systems used for the calculation of the dielectric function for Faraday ($\mathbf{B} \parallel [111]$) and for the Voigt configuration ($\mathbf{B} \parallel [1\bar{1}0]$) direction. The growth axis of the epitaxial film is along the [111] direction.

$$\epsilon^2(1,1) = -\frac{n^o_{90^\circ}e^2}{\epsilon_0\omega m_t}\frac{1}{\omega+i\omega_\tau},$$

$$\epsilon^2(2,2) = -\frac{n^o_{90^\circ}e^2}{\epsilon_0\omega m_t}\frac{\left(\frac{1}{9}+\frac{8}{9}\frac{m_t}{m_l}\right)(\omega+i\omega_\tau)}{\left[(\omega+i\omega_\tau)^2-\omega^2_{cA}\right]},$$

$$\epsilon^2(3,3) = -\frac{n^o_{90^\circ}e^2}{\epsilon_0\omega m_t}\frac{\left(\frac{8}{9}+\frac{1}{9}\frac{m_t}{m_l}\right)(\omega+i\omega_\tau)}{\left[(\omega+i\omega_\tau)^2-\omega^2_{cA}\right]}, \tag{9}$$

$$\epsilon^2(2,3) = -\frac{n^o_{90^\circ}e^2}{\epsilon_0\omega m_t}\frac{\left(-\frac{\sqrt{8}}{9}+\frac{\sqrt{8}}{9}\frac{m_t}{m_l}\right)(\omega+i\omega_\tau)+\frac{ieB}{m_l}}{\left[(\omega+i\omega_\tau)^2-\omega^2_{cA}\right]},$$

$$\epsilon^2(3,2) = -\frac{n^o_{90^\circ}e^2}{\epsilon_0\omega m_t}\frac{\left(-\frac{\sqrt{8}}{9}+\frac{\sqrt{8}}{9}\frac{m_t}{m_l}\right)(\omega+i\omega_\tau)-\frac{ieB}{m_l}}{\left[(\omega+i\omega_\tau)^2-\omega^2_{cA}\right]}.$$

The valleys 3 and 4 are oblique valleys with a carrier concentration determined by $n^o_{35^\circ}$. The ϵ^{34} tensor components are given by

$$\epsilon^{3,4}(1,1) = -\frac{n^o_{35^\circ}e^2}{\epsilon_0\omega m_t}\frac{1}{(\omega+i\omega_\tau)}\frac{(\omega+i\omega_\tau)^2\frac{1}{3}\left(1+2\frac{m_t}{m_l}\right)-\omega^2_{cA}}{\left[(\omega+i\omega_\tau)^2-\omega^2_{cB}\right]},$$

$$\epsilon^{3,4}(2,2) = -\frac{n^o_{35^\circ}e^2}{\epsilon_0\omega m_t}\frac{(\omega+i\omega_\tau)\left[\frac{7}{9}+\frac{2}{9}\frac{m_t}{m_l}\right]}{\left[(\omega+i\omega_\tau)^2-\omega^2_{cB}\right]},$$

$$\epsilon^{3,4}(3,3) = -\frac{n^o_{35^\circ}e^2}{\epsilon_0\omega m_t}\frac{(\omega+i\omega_\tau)\left[\frac{8}{9}+\frac{1}{9}\frac{m_t}{m_l}\right]}{\left[(\omega+i\omega_\tau)^2-\omega^2_{cB}\right]}, \tag{10}$$

$$\epsilon^{3,4}(2,3) = -\frac{n^o_{35^\circ}e^2}{\epsilon_0\omega m_t}\frac{(\omega+i\omega_\tau)\frac{\sqrt{2}}{9}\left(1-\frac{m_t}{m_l}\right)+ieB\frac{1}{3}\left(\frac{1}{m_l}+\frac{2}{m_t}\right)}{\left[(\omega+i\omega_\tau)^2-\omega^2_{cB}\right]},$$

$$\epsilon^{3,4}(3,2) = -\frac{n^o_{35^\circ}e^2}{\epsilon_0\omega m_t}\frac{(\omega+i\omega_\tau)\frac{\sqrt{2}}{9}\left(1-\frac{m_t}{m_l}\right)-ieB\frac{1}{3}\left(\frac{1}{m_l}+\frac{2}{m_t}\right)}{\left[(\omega+i\omega_\tau)^2-\omega^2_{cB}\right]}, \tag{11}$$

where

$$\omega_{cB} = eB\left(\frac{2m_l+m_t}{3m_tm_l}\right)^{1/2}. \tag{12}$$

C. Total dielectric function

1. *Faraday configuration*

For the Faraday configuration the total ϵ is given by[25]

$$\epsilon = 1+\chi_\infty+\chi_{\rm ph}+\chi^{\pm}_{\rm FC}, \tag{13}$$

where

$$\chi_{\rm ph} = \frac{(\epsilon_s-\epsilon_\infty)\omega^2_{\rm TO}}{\omega^2_{\rm TO}-\omega^2-i\omega\gamma}, \tag{14}$$

$\omega_{\rm TO}$ is the TO phonon frequency, ϵ_s and ϵ_∞ are the static and high frequency dielectric constant, and γ is the phonon damping parameter. For $\mathbf{B} \parallel [111]$ the two cyclotron resonance structures appear which manifest themselves in the transmission spectrum.

2. *Voigt configuration*

The total dielectric function for the ordinary mode is given by

$$\epsilon^o = \epsilon_{xx} = 1+\chi_\infty+\chi_{\rm ph}+\chi^{\rm FC}_{xx}. \tag{15}$$

For the extraordinary mode

$$\epsilon^e = \epsilon_{yy} - \frac{\epsilon_{yz}\epsilon_{zy}}{\epsilon_{zz}} \tag{16}$$

and hence

$$\epsilon^e = 1 + \chi_\infty + \chi_{\rm ph} + \chi_{yy}^{\rm FC} - \frac{(\chi_{yz}^{\rm FC}\chi_{zy}^{\rm FC})}{1 + \chi_\infty + \chi_{\rm ph} + \chi_{zz}^{\rm FC}}. \tag{17}$$

Resonantlike structures in ϵ^e cannot be simply associated with cyclotron resonances for the following reasons.

(i) Close to zeros in ϵ_{zz} resonant structures in $\tilde{n}_e^2$ occur.

(ii) One resonantlike structure occurs close to ω_{cB} and another one is a hybrid resonance which is observed at $\omega = \left(\omega_{cA}^2 + \omega_{cB}^2\right)^{1/2}$ for constant lattice contribution.

(iii) A plasma shifted cyclotron resonance occurs.

In addition to these commonly known resonances for light propagation parallel to the [111] direction, resonances also appear close to ω_{cA}, ω_{cB} and $\omega_{\rm TO}$, where the resonance near ω_{cB} is nearly canceled due to the structure of the total term $\epsilon_{yz}\epsilon_{zy}/\epsilon_{zz}$.

However, for laser photon energies $\hbar\omega$ close to the LO phonon mode frequency, very interesting cancellations appear within the imaginary part of the whole expression for ϵ^e. Since one of the FIR laser photon energies ($\lambda = 96.5$ μm) is close to $\omega_{\rm LO}$ of PbTe this situation is observed experimentally. In Fig. 7(a) the contribution of the several parts of the dielectric function are shown versus magnetic field. For this wavelength, at the resonant structure close to 3.5 T, the imaginary part of ϵ_{yy} and those of $\epsilon_{yz}\epsilon_{zy}/\epsilon_{zz}$ are nearly equal but of opposite sign. The same holds approximately for the real parts of both terms. In Fig. 7(b) the sensitivity of this cancellation of terms in the total dielectric function on the laser wavelength is shown. For longer laser wavelengths ($\lambda > 96.5$ μm) the resonant structure close to ω_{cB} appears again. The same is true for shorter laser wavelengths. This cancellation depends less critically on the carrier concentration because the number of carriers enters in ϵ_{zz} in the denominator as well. As a consequence one expects that for $\lambda = 96.5$ μm the resonant structure expected at about $B = 3.5$ T does not appear for the sample under investigation.

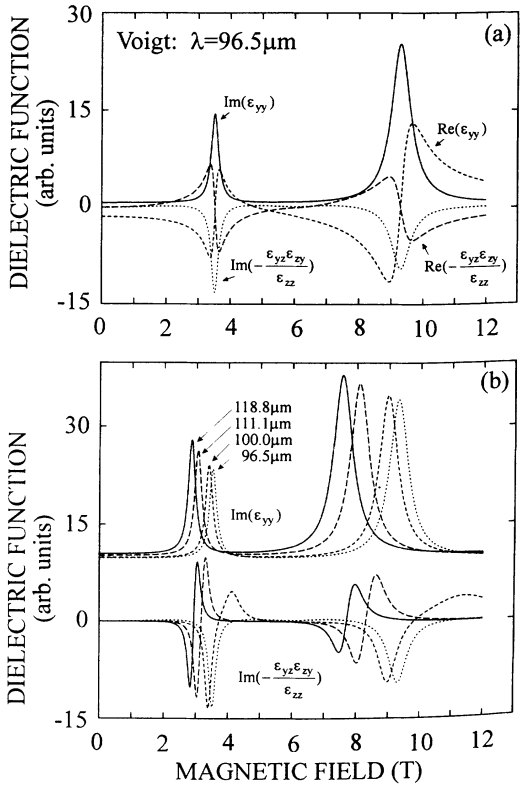

FIG. 7. (a) Calculated real (Re) and imaginary (Im) parts of the dielectric function for $\lambda = 96.5\mu$ as a function of the magnetic field for Voigt geometry ($\mathbf{B} \parallel [1\bar{1}0]$). Full line, Im ($\epsilon_{yy}$); dotted line, Im ($-\epsilon_{yz}\epsilon_{zy}/\epsilon_{zz}$), dashed lines, Re ($\epsilon_{yy}$) and Re ($-\epsilon_{yz}\epsilon_{zy}/\epsilon_{zz}$). For this laser wavelength the resonantlike structures [Imϵ_{yy}, Im$(-\epsilon_{yz}\epsilon_{zy}/\epsilon_{zz})$] close to $B = 3.5$ T nearly cancel each other. (b) Calculated imaginary parts Im(ϵ_{yy}) and Im$(-\epsilon_{yz}\epsilon_{zy}/\epsilon_{zz})$ as above, as a function of magnetic fields for four FIR wavelengths ($\lambda = 96.5$ μm, $\lambda = 100.0$ μm, $\lambda = 111.1$ μm, and $\lambda = 118.8$ μm) demonstrating that the cancellation of the two terms in the imaginary part of ϵ disappears for wavelengths $\lambda > 96.5$ μm.

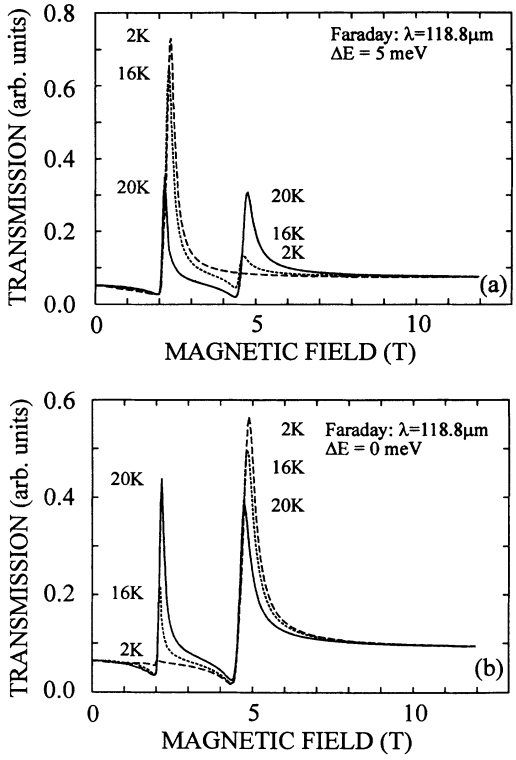

FIG. 8. Calculated magnetotransmission spectra in Faraday geometry ($\mathbf{B} \parallel [111]$) at a wavelength of $\lambda = 118.8$ μm as a function of temperature for two values of strain splitting: (a) $\Delta E = 5$ meV and (b) $\Delta E = 0$ meV. The size of the first dielectric anomaly following the cyclotron resonance in the [111] l valley is much larger for $\Delta E = 5$ meV than for $\Delta E = 0$ meV due to carrier transfer into the lowest lying level. For $\Delta E = 5$ meV the dielectric anomaly following the CR in the three o valleys becomes more pronounced for increasing temperature due to thermal population of the lowest Landau level of the three oblique valleys ($\omega_{\tau 1} = \omega_{\tau 2} = 4$ cm^{-1}).

To summarize the results of this section we show in Fig. 8 several calculated transmission spectra in Faraday configuration (**B** || [111]). In Fig. 8(a) the spectra are shown for a strain splitting between the l and o valleys of $\Delta E = 5$ meV and in Fig. 8(b) for 0 meV, respectively, with the lattice temperature as a parameter. Since for $\lambda = 118.8$ μm close to $B = 2$ T the cyclotron resonance within the l valleys is observed, the changes of their population with ΔE and temperature are clearly observable from the size of the dielectric anomaly associated with this cyclotron resonance.

In Fig. 9 calculated transmission spectra are shown for the Voigt configuration (**B** || [1$\bar{1}$0]) for a laser wavelength $\lambda = 96.5$ μm in order to demonstrate the changes caused by different values of the strain splitting energies $\Delta E = 0$ meV [Fig. 9(b)] and 5 meV [Fig. 9(a)]. A resonantlike structure which appears for $\Delta E = 0$ meV is absent for $\Delta E = 5$ meV slightly above $B = 3.5$ T.

IV. RESULTS AND ANALYSIS

A. Faraday configuration B || [111]

We compare experimental magnetotransmission data, Fig. 10(a), for $\lambda = 118.8$ μm obtained at three temperatures with model data, Fig. 10(b), based on the calculations presented in Sec. II, with the sample parameters and the band parameters listed in Table I. The strain-induced splitting was assumed to be $\Delta E = 1.5$ meV for Fig. 10(b), with a change only to $\Delta E = 1.0$ meV for the Fig. 10(b) inset. For the carrier damping parameters τ_1 and τ_2 values of 6 and 10 cm^{-1} were taken. At this laser wavelength $\hbar\omega$ lies below the energy of the longitudinal optical phonons, and thus the two cyclotron resonances in the l and o valleys are accompanied by dielectric anomalies which manifest themselves as an enhancement of the transmission for magnetic fields above the resonance fields. Note the large change in the temperature dependence of the first dielectric anomaly upon reduction of the strain splitting in the calculation to $\Delta E = 1.0$ meV, placing a lower bound on the strain energy for this sample.

Experimental data in Fig. 11(a) are compared with model calculations in Fig. 11(b) for a laser wavelength of $\lambda = 70.6$ μm, for which $\hbar\omega > \hbar\omega_{LO}$. Consequently, no dielectric anomalies appear and the transmission minima correspond to the cyclotron resonance fields for both types of valleys. For the calculated transmission data $\Delta E = 1.5$ meV, and $\tau_1 = \tau_2 = 10$ cm^{-1}.

B. Voigt configuration B || [1$\bar{1}$0]

In the following we show results for the magnetotransmission spectra taken with three FIR laser wavelengths

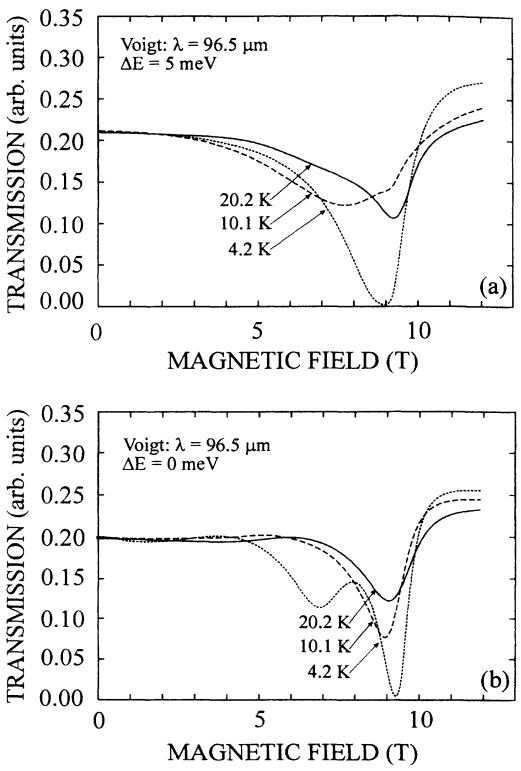

FIG. 9. Calculated magnetotransmission spectra at FIR laser wavelength $\lambda = 96.5$ μm for Voigt geometry (**B** || [1$\bar{1}$0]). Parameters used in the calculation are identical to those used in Fig. 8 [$\Delta E = 0$ in (a) and 5 meV in (b), and $n = 1 \times 10^{16}$ cm^{-3}].

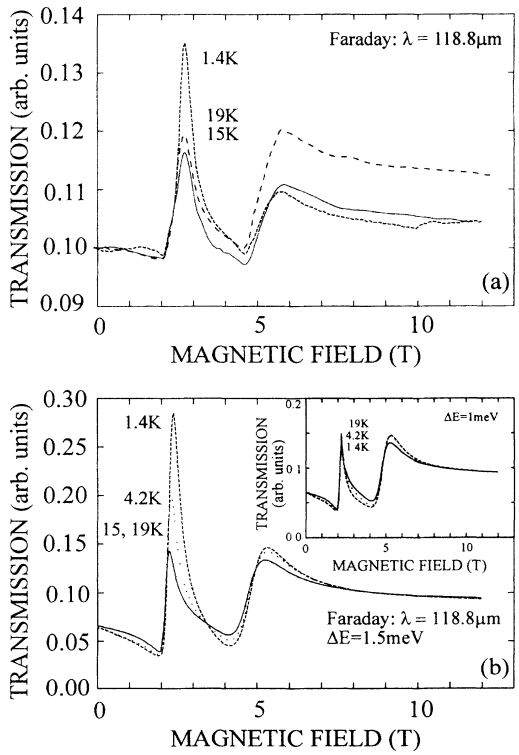

FIG. 10. Comparison of measured and calculated magnetotransmission curves for Faraday geometry **B** || [111] at $\lambda = 118.8$ μm. (a) Measured data for three temperatures. (b) Calculated data for $\Delta E = 1.5$ meV using $\omega_{\tau 1} = 6$ cm^{-1} and $\omega_{\tau 2} = 10$ cm^{-1} as free carrier damping parameters. Inset: calculated data using $\Delta E = 1.0$ meV, displaying the significant reduction in the temperature dependence of the first dielectric anomaly for a small change in strain splitting.

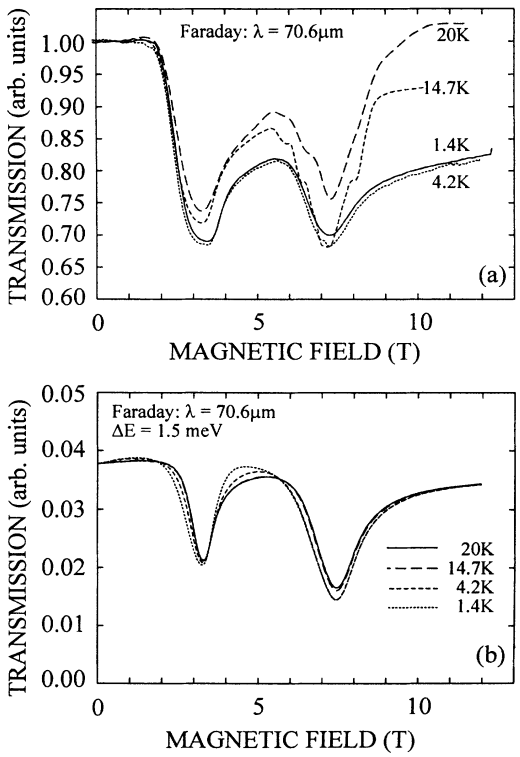

FIG. 11. Comparison of measured and calculated magnetotransmission curves as in Fig. 10 but with $\lambda = 70.6$ μm in Faraday geometry ($\mathbf{B} \parallel [111]$), and for four temperatures. (a) Measured magnetotransmission. (b) Calculated data using $\Delta E = 1.5$ meV, and $\omega_{\tau 1} = \omega_{\tau 2} = 10$ cm^{-1}.

$\lambda = 118.8$ μm, $\lambda = 96.5$ μm, and $\lambda = 70.6$ μm and for several temperatures. These data demonstrate that using the identical strain value of $\Delta E = 1.5$ meV as used for the calculated magnetotransmission spectra in Faraday configuration reasonable agreement with the observed FIR spectra is obtained.

In Fig. 12(a) the transmission data for $\lambda = 118.8$ μm are shown for four temperatures. For the first resonant-like structure (close to $B = 2.3$ T) the dip increases in strength with increasing temperature, whereas for the third one, the height of the structure decreases with increasing temperature. In the calculations [Fig. 12(b)] exactly this trend is observed. Experimentally an additional structure at about $B = 4$ T is observed which can be explained if in addition to ω_{cA} and ω_{cB} a spin-flip transition within the two valleys oriented by 35.26° with respect to $\mathbf{B} \parallel [1\bar{1}0]$ is introduced as an additional oscillator in the calculations. Consequently, with increasing temperature this structure becomes stronger.

Similar results for $\lambda = 70.6$ μm are shown in Figs. 13(a) and 13(b). Here the trends with the variation of the lattice temperature are much more pronounced than for the data for $\lambda = 118.8$ μm and again well accounted for by the calculated magnetotransmission spectra. The low temperature spectrum has been calculated for $\Delta E = 2.0$ meV as well as the 1.5 meV strain splitting and is shown in the inset to Fig. 13(b). Comparison of these strain splittings, separated by only 0.5 meV, illustrates that a splitting of 2.0 meV produces features too weak to account for the data, placing an upper bound on the strain splitting energy of this sample.

The magnetotransmission data for $\lambda = 96.5$ μm are shown in Figs. 14(a) and 14(b). Instead of the three features found for the two other wavelengths, Fig. 14(a) displays a single transmission minimum followed by a dielectric anomaly. For this FIR laser wavelength, the photon energy is quite close to the LO phonon energy and the cancellation of the terms in $\mathrm{Im}(\epsilon_{yy})$ and $\mathrm{Im}(-\epsilon_{yz}\epsilon_{zy}/\epsilon_{zz})$ predicted in Sec. III is indeed observed.

In Fig. 15 the FIR transmission in the ordinary Voigt geometry ($\mathbf{E} \parallel \mathbf{B}$) versus magnetic field from 11 T to 12 T is shown as a function of temperature for $\lambda = 118.8$ μm. In the inset, the dependence of the 0^- and 0^+ Landau states of the $\theta = 90°$ valley are shown. The strength of the spin-flip transition ($0^- \rightarrow 0^+$) weakens with increasing temperature exhibiting the effect of the thermal depopulation of the 0^- state of the [111] valley (see Fig. 3). Thus the temperature dependence of this spin-flip transition is an agreement with all previous statements on the occupancy of the various Landau states.

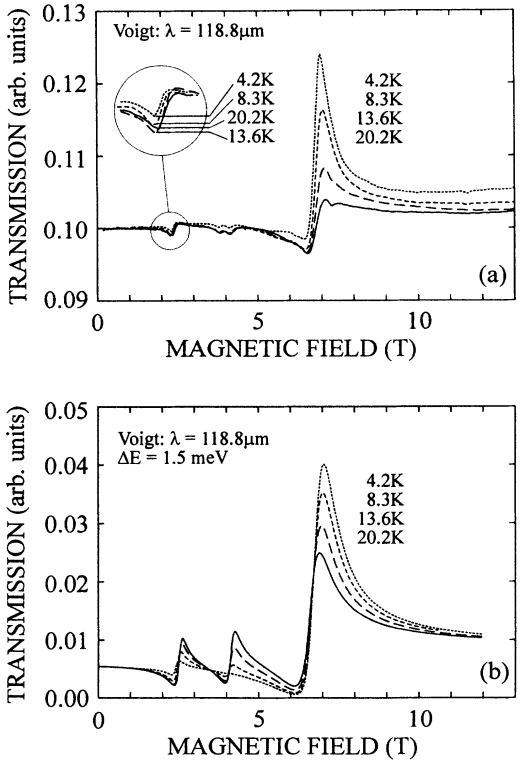

FIG. 12. Magnetotransmission in extraordinary Voigt geometry $\mathbf{B} \perp \mathbf{E}$, $\mathbf{B} \parallel [1\bar{1}0]$, $\mathbf{k} \parallel [111]$ with $\lambda = 118.8$ μm. (a) Measured data for four temperatures, with the inset showing detail of temperature dependence of first resonance structure. (b) Calculated data with $\Delta E = 1.5$ meV and all dampings $\omega_\tau = 4$ cm^{-1}. Resonant structures as described in the text. The first two structures increase in strength with increasing temperature and the third one decreases. Dominant terms for the first two are transitions within the oblique $\theta = 35.26°$ valleys, the second one originating from a spin-flip transition in these valleys ($\Delta E = 1.5$ meV).

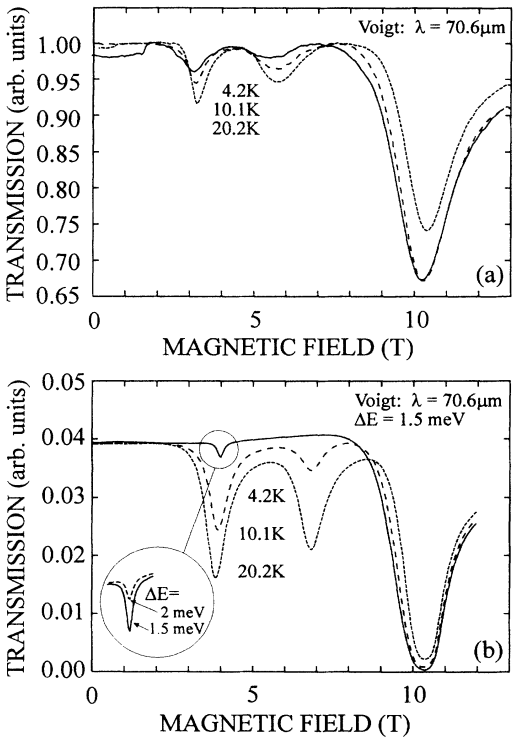

FIG. 13. Magnetotransmission in extraordinary Voigt geometry $\mathbf{B} \perp \mathbf{E}$, $\mathbf{B} \parallel [1\bar{1}0]$, $\mathbf{k} \parallel [111]$ as in Fig. 12 but for $\lambda = 70.6$ μm. (a) is measured spectra and (b) is the model calculation using $\Delta E = 1.5$ meV and $\omega_\tau = 4$ cm^{-1}.

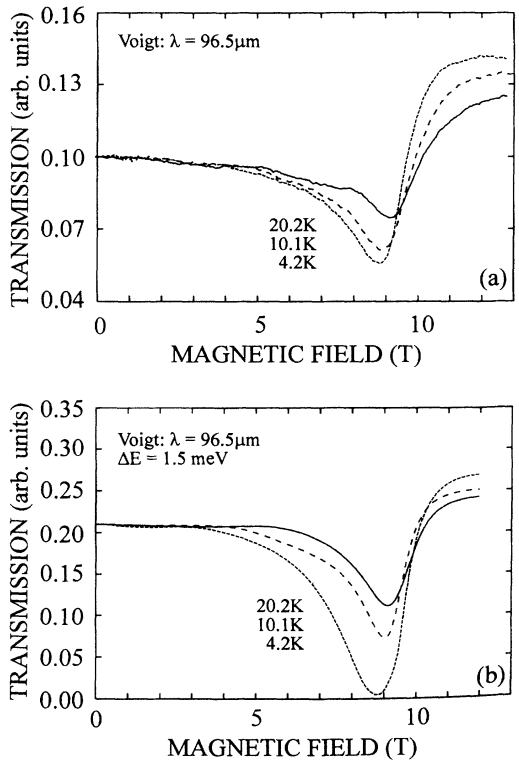

FIG. 14. Magnetotransmission in extraordinary Voigt geometry $\mathbf{B} \perp \mathbf{E}$, $\mathbf{B} \parallel [1\bar{1}0]$, $\mathbf{k} \parallel [111]$ as in Fig. 12 but for $\lambda = 96.5$ μm. (a) is measured data and (b) the model calculation. The temperature dependence of the resonant structure close to $B = 9$ T reflects the depopulation of the $\theta = 90°$ valleys 0^- Landau levels with increasing temperature. For the parameters used for the calculation see the main text. The main feature is the disappearance of the first and second resonant structure for this laser photon energy close to $\hbar\omega_{LO}$. ($\Delta E = 1.5$ meV.)

V. CONCLUSION

Far infrared magnetotransmission experiments have been performed on a high mobility PbTe layer grown epitaxially on a (111) oriented BaF_2 substrate. From a detailed analysis of the experimental data which were taken in Faraday ($\mathbf{B} \parallel [111]$) and Voigt ($\mathbf{B} \parallel [1\bar{1}0]$) geometries for temperatures in the range 1.4–20 K, the amount of strain splitting between the four $\langle 111 \rangle$ valleys has been obtained. In Voigt geometry spin-flip transitions were observed in addition to resonances associated with cyclotron resonances. It was shown that a complicated fitting procedure based on a complete dielectric function is necessary for a quantitative understanding of the various transmission features which change in their respective strength as a function of laser wavelength and with temperature. These changes reflect the varying occupancy as functions of magnetic field and temperature of Landau states associated with the valleys oriented either parallel or oblique to the growth direction. In addition, they depend sensitively on the amount of biaxial tensile strain present in the epilayer, which splits the energy minima of the longitudinal and oblique valleys by ΔE. For the Voigt configuration ($\mathbf{B} \parallel [1\bar{1}0]$) the presence of biaxial strain splits even the otherwise equivalent two $\theta = 90°$ valleys. The value of ΔE is obtained as the decisive fit parameter (apart from fitting phenomenological broadening parameters of the magneto-optical transitions). Specifically, Faraday transmission data at $\lambda = 118.8$ μm places a

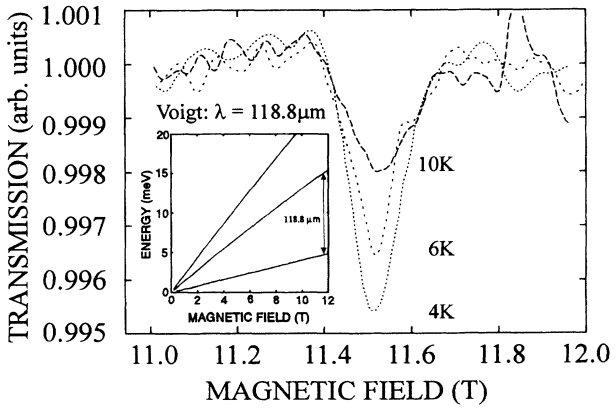

FIG. 15. Temperature dependence of magnetotransmission in ordinary Voigt geometry $\mathbf{B} \parallel \mathbf{E}$, $\mathbf{B} \parallel [1\bar{1}0]$, $\mathbf{k} \parallel [111]$, showing a transmission minimum close to $B = 11.5$ T for $\lambda = 118.8$ μm due to a spin-flip transition ($0^- \rightarrow 0^+$) in the lowest lying $\theta = 90°$ valley. Its temperature dependence reflects the decreasing population of this valley with increasing temperature.

lower bound and Voigt transmission data at $\lambda = 70.6$ μm places an upper bound on the strain splitting energy of $\Delta E = 1.5 \pm 0.25$ meV used in the model calculations for this sample.

An interesting cancellation of terms in the magnetic-field dependence of the dielectric function in Voigt configuration is predicted and observed by the absence of a resonantlike structure in our experimental data in the extraordinary Voigt mode. The effect is due to the proximity of the LO phonon energy of PbTe (14 meV) to the photon energy of one of the FIR laser lines used ($\lambda = 96.5$ μm) and is explained quantitatively.

ACKNOWLEDGMENTS

This work was supported by Fonds zur Fürderung der Wissenschaftlichen Forschung Project No. 8250 PHY and by National Science Foundation Grant No. INT-9014015. We thank J. Furneaux for help with the FIR experiments and H. Clemens for the sample growth.

[1] D. L. Partin, IEEE J. Quantum Electron. **QE-24**, 1716 (1988).
[2] A. Lopez-Otero, Thin Solid Films **49**, 5 (1978).
[3] H. Holloway, *Physics of Thin Films*, edited by G. Hass and M. H. Francombe (Academic Press, New York, 1980), p. 5.
[4] R. F. Bis, J. R. Dixon, and J. R. Lowney, J. Vac. Sci. Technol. **9**, 226 (1972).
[5] D. L. Mitchell and R. F. Wallis, Phys. Rev. **151**, 581 (1966).
[6] J. O. Dimmock, in *The Physics of Semimetals and Narrow Band Semiconductors*, edited by D. L. Carter and R. T. Bate (Pergamon, Oxford, 1971), p. 405.
[7] J. B. Restorff, R. S. Allgaier, and B. Houston, J. Appl. Phys. **52**, 6185 (1981).
[8] J. B. Restorff, R. S. Allgaier, and B. Houston, J. Appl. Phys. **53**, 3115 (1982).
[9] J. R. Burke and G. P. Carver, Phys. Rev. B **17**, 2719 (1978).
[10] J. Oswald, B. B. Goldberg, G. Bauer, and P. J. Stiles, Phys. Rev. B **40**, 3032 (1989).
[11] W. Weber and K. F. Yeung, J. Appl. Phys. **44**, 4991 (1973).
[12] E. Bangert, G. Bauer, E. J. Fantner, and H. Pascher, Phys. Rev. B **31**, 7958 (1985).
[13] S. W. McKnight and H. D. Drew, Phys. Rev. B **21**, 3447 (1980).
[14] S. Perkowitz, Phys. Rev. **182**, 828 (1969).
[15] H. Ch. Schaber and R. E. Doezema, Phys. Rev. B **20**, 5257 (1979).
[16] T. Ichiguchi, S. Nishikawa, and K. Murase, Solid State Commun. **34**, 309 (1980).
[17] B. B. Goldberg, J. E. Furneaux, J. Oswald, G. Bauer, and P. J. Stiles, Semicond. Sci. Technol. **5**, S151 (1990).
[18] H. Burkhard, G. Bauer, and W. Zawadzki, Phys. Rev. B **19**, 5149 (1979).
[19] A. Krost, B. Harbecke, R. Faymonville, H. Schlegel, E. J. Fantner, K. E. Ambrosch, and G. Bauer, J. Phys. C **13**, 561 (1985).
[20] J. Singleton, E. Kress-Rogers, A. V. Lewis, R. J. Nicholas, E. J. Fantner, and A. Lopez-Otero, J. Phys. C **19**, 77 (1986).
[21] E. J. Fantner, H. Clemens, and G. Bauer, in *Advances in X-Ray Analysis*, edited by J. B. Cohen, J. C. Russ, D. E. Leyden, C. S. Barrett, and P. K. Predecki (Plenum, New York, 1984), Vol. 27, p. 171.
[22] A. E. Asch, D. Gorski, D. K. Hohnke, H. Holloway, M. D. Hurley, E. T. Hutcheson, S. W. Kaiser, P. V. S. Rao, and A. J. Varga (unpublished).
[23] G. Bauer, in *Narrow Gap Semiconductors: Physics and Applications*, edited by W. Zawadzki, Springer Lecture Notes in Physics Vol. 133 (Springer-Verlag, Berlin, 1980), p. 427.
[24] M. S. Adler, C. R. Hewes, and S. D. Senturia, Phys. Rev. B **7**, 186 (1973).
[25] G. Bauer, in *Landau Level Spectroscopy*, edited G. Landwehr and E. I. Rashba (Elsevier Science Publishers B.V., Amsterdam, 1991), Vol. 1, p. 277.
[26] E. D. Palik and J. K. Furdyna, Rep. Prog. Phys. **33**, 1193 (1970).
[27] G. Karczewski, J. K. Furdyna, D. L. Partin, C. N. Trush, and J. Heremans, Phys. Rev. B **46**, 13 331 (1992).
[28] G. Bauer, H. Pascher, and W. Zawadzki, Semicond. Sci. Techno. **7**, 703 (1992).